Determination of misalignment and angular scale errors of a laser tracker using a new geometric model and a multi-target network approach

Andrew Lewis[1] , Ben Hughes[1], Alistair Forbes[1], Wenjuan Sun[1], Dan Veal[1], Karim Nasr[1]

[1]*National Physical Laboratory, Hampton Road, Teddington, Middlesex, TW11 0LW, United Kingdom*

Corresponding author: Andrew Lewis

Abstract

We report on the determination of laser tracker geometrical alignment and angular scale errors using a new geometric error model and repeated measurements of a network of fixed targets which are measured using a laser tracker, mounted in five different locations/orientations. After fitting to the data, we are able to determine geometrical/angular scale errors of the tracker with sufficient accuracy that a previously un-calibrated tracker can easily pass a standard performance verification test, after being error-mapped using our technique. Our technique uses no special equipment, takes under one hour and provides rigorous uncertainty values for the error parameters.

1 Introduction

The invention of the tracking laser interferometer [1], or *laser tracker,* combined the displacement measuring accuracy of a laser interferometer with the three-dimensional angular measuring capability of a theodolite or total-station, to produce a measuring instrument capable of high accuracy, long range 3-D metrology. Laser trackers have become the most accurate metrology tool for use in large volume dimensional metrology and their use is widespread within several industries such as aerospace, surveying, automotive manufacture, civil engineering and large-scale engineering. Conceptually, a laser tracker is a portable coordinate measuring system that obtains data in a spherical polar coordinate system, making measurements of a distance (range) and two angles (d, θ, ϕ). The laser tracker uses a target displacement sensor and motorised gimbal mechanism to steer the laser beam to track a moving target, which is usually a spherically mounted retro-reflector (SMR). The two rotation angles of the gimbal are measured by precision angle encoders mounted on the mechanism to provide azimuth, θ, and elevation, ϕ, angles to the target. Simultaneously, the radial distance to the target, or range component, d, is measured by an interferometer (IFM) or an absolute distance meter (ADM). The range measurement is corrected for refractive index of the ambient air [2] using measured values of the air temperature, pressure and assumed humidity.

In the same way that a conventional Cartesian coordinate measuring machine (CMM) is subject to a series of geometrical errors [3], the performance of a laser tracker is degraded by misalignments, offsets, non-linearities and eccentricities of the beam steering mechanism and of the angular encoders within the laser tracker, leading to errors in the measured coordinates. In order to compensate for these errors, laser tracker manufacturers provide online correction of systematic effects using software algorithms running on the tracker controller system. The correction software relies on a model that describes the beam steering mechanism and its errors. The parameters of the model are usually derived from a series of measurements performed either by the manufacturer (when the tracker is manufactured) or by the user (prior to each use of the instrument).

End-user measurements are only able to determine a subset of all the error parameters – typically linear offsets of the ranging system origin, rotation axis offsets and axis misalignments. Only the measurements performed by the manufacturer are used to determine the angular scale errors, with the assumption being that these do not vary over short to medium timescales, and thus do not require end-user correction. A disadvantage of the techniques used for end-user measurement of geometrical errors is that the measurements determine only parameter values but with no uncertainty estimation. The user is therefore unable to decide if the process is accurate enough for their intended use of the tracker, and

is not able to propagate those uncertainties through to subsequent measurements made using the laser tracker; a pre-requisite for traceability.

To address these issues, we designed an alternative measurement procedure that is able to determine *all* the alignment and angle encoder errors of a laser tracker and their corresponding uncertainties, *simultaneously*. In order to make this user-friendly, we designed the procedure to require no specialist equipment and optimised the process such that a user can perform it in less than an hour. The procedure is derived from the concept of multilateration [4] in which multiple measurements of the same target, from various locations, are used to improve the target measurement accuracy. In our technique, we use multiple measurements of a series of fixed target locations (SMR nests), with all the measurements made using the same laser tracker, with the tracker moved to a different position for each set of measurements.

After data acquisition, we perform a least-squares fit to the data, to locate the tracker positions and target positions in space. Essentially, we regard the errors remaining in the fitted tracker and target positions after the bundle adjustment as being the result of the tracker geometrical errors so we simultaneously fit a mathematical error model of the tracker to the observations, in order to determine the parameters of the model, as well as their uncertainties. To obtain the most accurate data, the measurements are made in IFM mode and we include measurements in both front face and back face mode of the tracker, *i.e.* we use two-face[1] measurements.

2 Error model

2.1 Idealised laser tracker

An idealised laser tracker is shown schematically in figure 1. The two rotation axes are orthogonal and intersect at a point, taken to be the origin of the spherical polar coordinate system. The laser beam origin is also located at the intersection of the two axes and the initial beam direction is normal to the transit axis. The two angular encoders are mounted such that each is coaxial with the respective rotation axis, and each encoder is assumed to have a scale of uniform pitch, aligned radially with the centre of rotation of the axis.

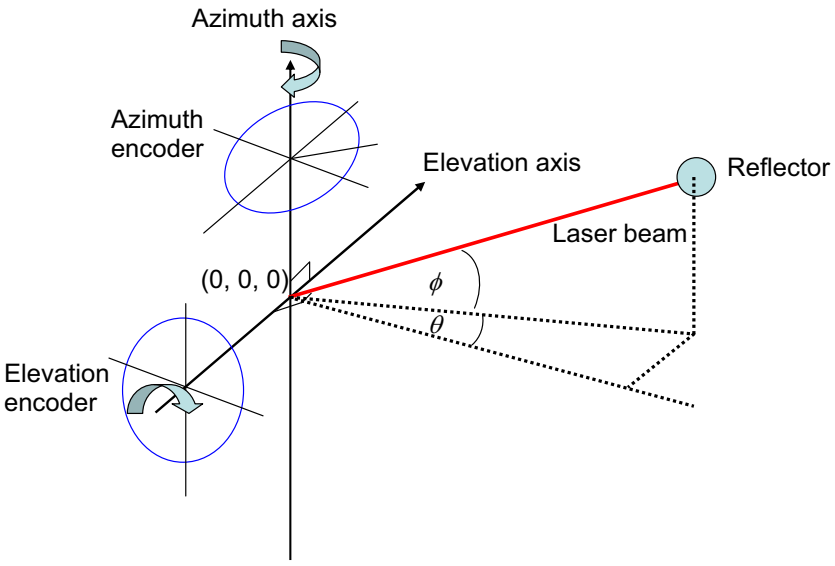

Figure 1. Schema of an idealised laser tracker.

[1] The term 'two-face' refers to two measurements of the same target point – one with the tracker gimbals oriented conventionally ('front face'), the second with the azimuth axis rotated 180° and the elevation axis rotated to re-target the same point ('back face'). During the movement between the two orientations, the tracker rotates and inverts the laser head or targeting mirror. The nomenclature of the axes is given in figure 1.

2.2 Our new error model - error sources in a real tracker

In a real laser tracker, a series of imperfections are present, due to manufacturing tolerances and design constraints, and these can be conceptualised as a series of error parameters which are shown pictorially in figure 2, labelled in table 1 and described below.

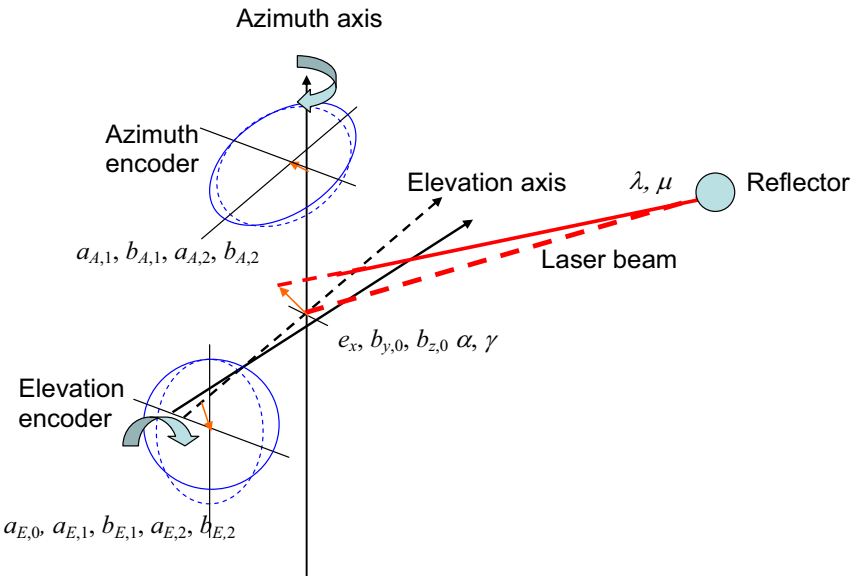

Figure 2. Error parameters of a real laser tracker.

Table 1. Error parameters and their physical origin. The index, *i*, refers to parameter **h** in equation (10).

i	**Parameter**	**Description**	**Type**
-	λ	range offset	distance
-	μ	scale factor for range	value
1	e_x	elevation (E) axis offset from azimuth (A) axis	distance
2	$b_{y,0}$	beam offset (y-direction) from origin	distance
3	$b_{z,0}$	beam offset (z-direction) from origin	distance
4	α	azimuth axis angle in yz-plane	angle
5	γ	beam axis angle in xy-plane	angle
6	$a_{A,1}$	azimuth scale error, first order Fourier term	angle
7	$b_{A,1}$	azimuth scale error, first order term Fourier term	angle
8	$a_{A,2}$	azimuth scale error, second Fourier term	angle
9	$b_{A,2}$	azimuth scale error, second Fourier term	angle
10	$a_{E,0}$	elevation angle offset	angle
11	$a_{E,1}$	elevation scale error, first Fourier term	angle
12	$b_{E,1}$	elevation scale error, first Fourier term	angle
13	$a_{E,2}$	elevation scale error, second Fourier term	angle
14	$b_{E,2}$	elevation scale error, second Fourier term	angle

These sixteen errors may be classified as: gimbal axis offsets and alignment errors (e_x, α, γ, $a_{E,0}$), beam origin errors (λ, μ, $b_{y,0}$, $b_{z,0}$), and angular scale errors ($a_{A,1}$, $b_{A,1}$, $a_{A,2}$, $b_{A,2}$, $a_{E,1}$, $b_{E,1}$, $a_{E,2}$, $b_{E,2}$). In our analysis, we limit the angular scale error terms to second order, though our model uses a Fourier

expansion of these terms (see equations 4 and 5) and could be easily extended to higher orders, if necessary. Our model contains an additional parameter, $a_{A,0,}$ but we set this equal to zero (see discussion below) so it does not appear in table 1.

2.3 New error model coordinate system

Before we describe the new error model in detail, we establish our model coordinate system and label the necessary components of the tracker. We have described this elsewhere [5, 6] but reiterate here for ease of reference. 'True' values of the coordinates (*i.e.* those predicted after application of the error model) are denoted with a star, *e.g.* θ^*, measured values are denoted without a star, *e.g.* θ. We assume that the measured values are subject to both systematic and randomly varying errors.

The azimuth axis of the tracker is the axis pointing nominally vertically and about this axis, the angular encoder measures an azimuth angle, θ. The elevation axis is nominally normal to the azimuth axis, and its angular encoder measures an elevation angle, ϕ. The azimuth axis is hereby labelled *A*, the elevation axis *E* and the laser beam axis *B*. We now relate the coordinate system of the laser tracker to a conventional Cartesian coordinate system. We define that *A* is aligned with the Cartesian *z*-axis. This alignment sets four frame of reference constraints, leaving two degrees of freedom, namely rotation around the *z*-axis and height along the *z*-axis.

We assume also that when $\theta^* = \phi^* = 0$, the axis *E* lies in a plane parallel to the *yz*-plane, thereby fixing the rotation about the *z*-axis, and also that it intersects the *x*-axis, thus fixing the height along the *z*-axis.

We further assume that when $\theta^* = \phi^* = 0$, *B* lies in a plane parallel to the *xy*-plane and that the beam source is at $\mathbf{b}_0$, nominally at the origin of both coordinate systems, and nominally pointing along the direction of the *x*-axis. With these assumptions, for $\theta^* = \phi^* = 0$, the azimuth axis *A* is given by the location point $(0,0,0)^T$ and direction vector $(0,0,1)^T$, and the elevation axis *E* is given by location point $\boldsymbol{e}_0$ and direction vector $\mathbf{n}_{E,0}$ with

$$\mathbf{e}_0 = \begin{bmatrix} e_{x,0} \\ 0 \\ 0 \end{bmatrix}, \quad \mathbf{n}_{E,0} = R_x(\alpha)\begin{bmatrix} 0 \\ 1 \\ 0 \end{bmatrix} \approx \begin{bmatrix} 0 \\ 1 \\ \alpha \end{bmatrix} \tag{1}$$

and *B* is given by location point $\mathbf{b}_0$ and direction vector $\mathbf{n}_{B,0}$ given by

$$\mathbf{b}_0 = \begin{bmatrix} b_{x,0} \\ b_{y,0} \\ b_{z,0} \end{bmatrix}, \quad \mathbf{n}_{B,0} = R_z(\gamma)\begin{bmatrix} 1 \\ 0 \\ 0 \end{bmatrix} \approx \begin{bmatrix} 1 \\ \gamma \\ 0 \end{bmatrix} \tag{2}$$

where we use short form notations $R_x(\alpha)$, $R_y(\beta)$ and $R_z(\gamma)$ for the Cartesian plane rotation matrices

$$R_x(\alpha) = \begin{bmatrix} 1 & 0 & 0 \\ 0 & \cos\alpha & -\sin\alpha \\ 0 & \sin\alpha & \cos\alpha \end{bmatrix}, R_y(\beta) = \begin{bmatrix} \cos\beta & 0 & \sin\beta \\ 0 & 1 & 0 \\ -\sin\beta & 0 & \cos\beta \end{bmatrix}, R_z(\gamma) = \begin{bmatrix} \cos\gamma & -\sin\gamma & 0 \\ \sin\gamma & \cos\gamma & 0 \\ 0 & 0 & 1 \end{bmatrix}$$

The parameters α and γ represent angular alignment errors of the laser tracker gimbals; α represents the angle of the transit axis in the *yz*-plane and γ represents the beam axis angle in the *xy*-plane. These are summarised, with other parameters, in figure 3.

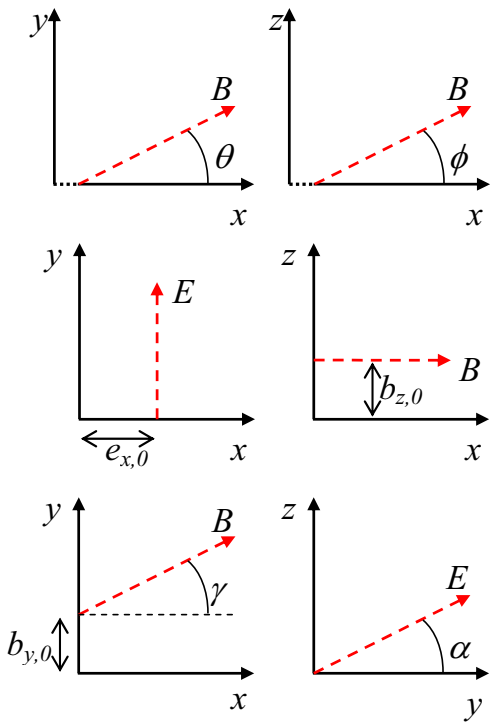

Figure 3. Linear and angular offset parameters. Parameter $b_{x,0}$ is defined to be zero so is not shown.

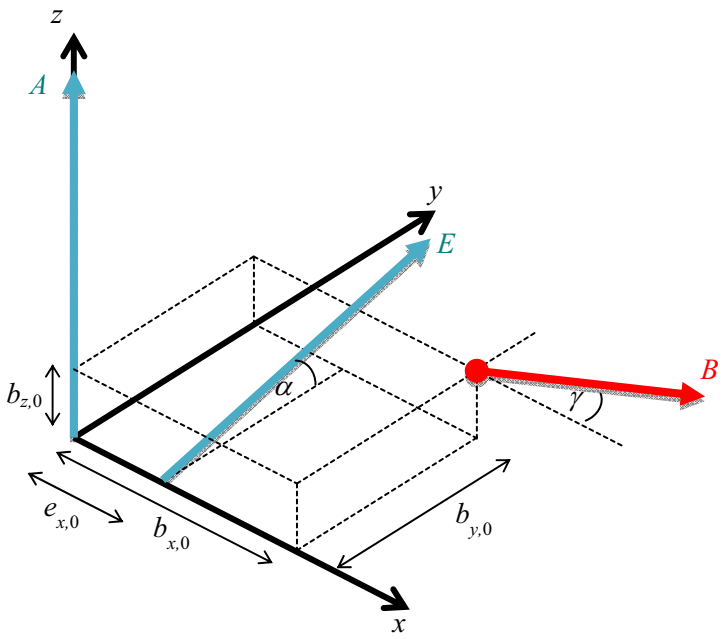

Figure 4. Isometric view of coordinate system. ($\theta = \phi = 0$).

We assume that the observed values d, θ, and ϕ for each target point are related to their true values d^*, θ^*, and ϕ^* according to the model equations (3) to (5).

$$d = (1+\mu)d^* + \lambda + e_D \tag{3}$$

$$\theta = \theta^* + a_{A,0} + \sum_{q=1}^{n_Q}\left[a_{A,q}\cos q\theta^* + b_{A,q}\sin q\theta^*\right] + e_A \tag{4}$$

$$\phi = \phi^* + a_{E,0} + \sum_{q=1}^{n_Q}\left[a_{E,q}\cos q\phi^* + b_{E,q}\sin q\phi^*\right] + e_E \tag{5}$$

Here, μ represents a scale correction (*e.g.* for refractive index), λ represents a displacement offset (*e.g.* laser dead-path), q represents the harmonic order of the Fourier series (maximum n_Q), which is used to represent the angle encoder errors such as eccentricity and scale. The parameters e_D, e_A and e_E are samples from a statistical distribution with expectation value zero and standard deviations σ_D, σ_A and σ_E, respectively (*i.e.* they represent random noise). Parameter $a_{A,0}$ is associated with fixing a frame of reference and is constrained to be zero (essentially this is an angular zero offset on the azimuth scale, but this only affects the global rotation of our coordinate system and has no effect on the geometrical errors of the model). Parameter $a_{E,0}$ cannot be arbitrarily constrained (it is the erroneous reading in the elevation angle when the laser beam is horizontal) and so remains in our model.

The x-component of $\mathbf{b}_0$, $b_{x,0}$, can be compensated by changing the offset parameter λ, so we constrain $b_{x,0}$ instead to be zero, *i.e.* we combine these two offsets into λ. This is similar to what is performed in practice when determining the range offset value for the tracker such that the zero point is located at the intersection of the axes. In reality this may not be the case: the laser beam may emerge from a location in front of or behind the axes intersection, and the interferometer or ADM zero point may not be coincident with the beam aperture, but these are two linear offsets that can be combined into one value such that the beam appears to have an origin at the axes intersection point.

Examination of equations (1) through (5), shows that the remaining error model parameter terms which are non-zero are $e_{x,0}$, $b_{y,0}$, $b_{z,0}$, α, γ, $a_{E,0}$ and the other $4n_Q$ Fourier terms. From several series of measurements made in a well-controlled laboratory environment, we determined that it is sufficient to limit the angular encoder error terms to second order and so we set $n_Q = 2$.

Equations (3–5) model how observations d, θ, and ϕ are generated given the true values d^*, θ^*, and ϕ^*. The model is completed by describing d^*, θ^*, and ϕ^* in terms of the position of the tracker, the locations of the targets and the alignment and encoder errors. We first consider the rotations of the tracker axes required to point the laser at any particular target.

At azimuth angle θ^*, the transit axis E is moved to a position specified by the transformed location point $\mathbf{e}$ and direction vector $\mathbf{n}_E$

$$\mathbf{e} = R_z(\theta^*)\mathbf{e}_0, \quad \mathbf{n}_E = R_z(\theta^*)\mathbf{n}_{E,0} = R_z(\theta^*)R_x(\alpha)\begin{bmatrix}0\\1\\0\end{bmatrix} \tag{6}$$

If a point $\mathbf{z}$ is rotated by ϕ^* about the axis E, it is moved to

$$\hat{\mathbf{z}} = \mathbf{e} + R_E(\mathbf{z}-\mathbf{e})$$

Where the rotation matrix R_E that corresponds to a rotation through angle ϕ^* about the transit axis E is given by

$$R_E(\theta^*,\phi^*) = R_z(\theta^*)R_x(\alpha)R_y(-\phi^*)R_x(-\alpha)R_z(-\theta^*) \tag{7}$$

Applying this transformation to $R_z(\theta^*)\mathbf{b}_0$, the laser beam source $\mathbf{b}_0$ is rotated by θ^* and ϕ^* to

$$\mathbf{b}(\theta^*,\phi^*) = \mathbf{e} + R_E\left(\theta^*,\phi^*\right)\left[R_z(\theta^*)\mathbf{b}_0 - \mathbf{e}\right]$$

$$\mathbf{b}(\theta^*,\phi^*) = R_z(\theta^*)\mathbf{e}_0 + R_z(\theta^*)R_x(\alpha)R_y(-\phi^*)R_x(-\alpha)(\mathbf{b}_0 - \mathbf{e}_0) \tag{8}$$

and the beam direction vector $\mathbf{n}_{B,0}$ is rotated to

$$\mathbf{n}_B(\theta^*,\phi^*) = R_E R_z(\theta^*)\mathbf{n}_{B,0}$$

$$\mathbf{n}_B(\theta^*,\phi^*) = R_z(\theta^*)R_x(\alpha)R_y(-\phi^*)R_x(-\alpha)R_z(\gamma)\begin{bmatrix}1\\0\\0\end{bmatrix} \tag{9}$$

Equations (8) and (9) give the physical origin and pointing direction of the laser beam, based on true values of the azimuth and elevation angles (θ^* and ϕ^*) and the beam and transit axis alignment offsets (α and γ). Combining equations (3, 4, 5, 8, 9) and letting $\mathbf{h}$ be the vector of $(6 + 4n_Q)$ geometric error model parameters, then for any target location $\mathbf{x}_i$,

$$\mathbf{x}_i = \mathbf{b}\left(\theta_i^*, \phi_i^*, \mathbf{h}\right) + d_i^*\mathbf{n}_B\left(\theta_i^*, \phi_i^*, \mathbf{h}\right) \tag{10}$$

There are two solutions of equation 10: if (θ^*,ϕ^*) are solution parameters, then there is also a solution close to $(\theta^*+\pi, \pi - \phi^*)$. These two solutions correspond to the front-face and back-face measurement modes of the tracker, as described previously.

Equation (10) defines d^*, θ^*, and ϕ^* as functions of $\mathbf{x}$ and of the geometric error parameters in the vector $\mathbf{h}$. Iterative techniques can therefore be used to solve (10) for d^*, θ^*, and ϕ^*, given starting estimates derived from nominal tracker geometry, such as $e_{x,0} = \alpha = \gamma = 0$, $\mathbf{b}_0 = (0,0,0)^T$. Table 1 summarises the individual parameters, $\mathbf{h}_i$, contained in $\mathbf{h}$, as well as the additional parameters λ and μ which determine d^*.

2.4 Using the new error model in a multi target network

As described in [5, 6], the error model parameters can be estimated from the measurement of a fixed set of targets $\mathbf{x}_j$, $j = 1, \ldots, n_X$ from a number of tracker positions determined by locations $\mathbf{p}_k$ and initial pointing directions $\boldsymbol{\alpha}_k$, with $k = 1, \ldots, n_S$. If d_i, θ_i, and ϕ_i are measurements associated with the j^{th} target and the k^{th} tracker position, then d_i^*, θ_i^*, and ϕ_i^* are determined by the the multi-station form of equation (10)

$$R(\boldsymbol{\alpha}_k)R_0(\mathbf{x}_j - \mathbf{p}_k) = \mathbf{b}(\theta_i^*,\phi_i^*,\mathbf{h}) + d_i^*\mathbf{n}_B(\theta_i^*,\phi_i^*,\mathbf{h}) \tag{11}$$

We allow for *l*-multiple resets of the range offset, λ, and for *r*-multiple scale correction parameters, μ. $R_0(\mathbf{x}_j - \mathbf{p}_k)$ is a fixed rotation matrix associated with the k^{th} measuring station (with respect to the frame of the target network) and R is the overall general rotation matrix formed as the product $R_z(\alpha)R_y(\beta)R_x(\gamma)$ of plane rotation matrices and describes the rotational mis-alignment angles of the k^{th} measuring station.

This leads to multi-station model equations which are derived from equations (3, 4, 5). We let **c** be the vector of all the configuration parameters $\mathbf{p}_k$, $\boldsymbol{\alpha}_k$, λ_l, μ_r and **h**, and set relative weights $w_{D,i} = 1/\sigma_{D,i}$, *etc*. We then solve the nonlinear least squares problem to determine the best estimator parameters

$\tilde{d}_i, \tilde{\theta}_i, \tilde{\phi}_i$

$$\min_{\{\mathbf{x}_j\},\mathbf{c}} \sum_i \left\{ w_{D,i}^2 (d_i - \tilde{d}_i(\mathbf{x}_j, \mathbf{c}))^2 + w_{A,i}^2 (\theta_i - \tilde{\theta}_i(\mathbf{x}_j, \mathbf{c}))^2 + w_{E,i}^2 (\phi_i - \tilde{\phi}_i(\mathbf{x}_j, \mathbf{c}))^2 \right\} + (B\mathbf{c} - \mathbf{c}_0)^{\mathrm{T}} (B\mathbf{c} - \mathbf{c}_0)$$

subject to certain reference constraints applied to **c** [7, 8, 9] and noting that the solution of the problem represents the maximum likelihood estimate of the parameters. We include an additional term, $B\mathbf{c} - \mathbf{c}_0$ to account for any additional prior information about the configuration paramaters, *e.g.* estimates of μ_r. We can therefore determine the uncertainties of the fitted parameters $\{\mathbf{x}_j\}$ and **c** by simple propagation from the observation uncertainties.

2.5 Using the model and the model parameters

The least squares solution produces estimates, **h**, of the error model parameters and a matrix V_{h} of the variances. These error parameter estimates, along with λ and μ, can be used to correct target estimates in the subsequent use of the tracker. This allows us to either compensate for small residual errors of a tracker that is using existing compensation values, or to use the parameters and the new geometric error model as a means of error mapping and compensating a laser tracker with no prior error model or active compensation.

3 Error correcting a commercial laser tracker

3.1 Performance test of an un-corrected laser tracker

In order to demonstrate the power of the technique, we used it to perform full error correction of a commercial laser tracker. We temporarily disabled the parameters of the tracker's error map (the map was a combination of manufacturer determined values and values from the latest user tests). Using the tracker's interferometer, we performed the IFM volumetric tests prescribed in standard ASME B89.4.19 [10]. (Other performance verification standards have since been developed [11, 12] but they share the same essential testing philosophy). These tests took two hours to complete. The results are shown graphically in figure 5, which shows deviation from calibrated artefact length, for a series of measurements of the artefact, using several locations and orientations of both the tracker and the artefact. Length measurement errors of up to 1.9 mm can be observed which are far in excess of the 18 µm to 68 µm maximum permissible error (MPE) values specified by the manufacturer for a properly operating tracker.

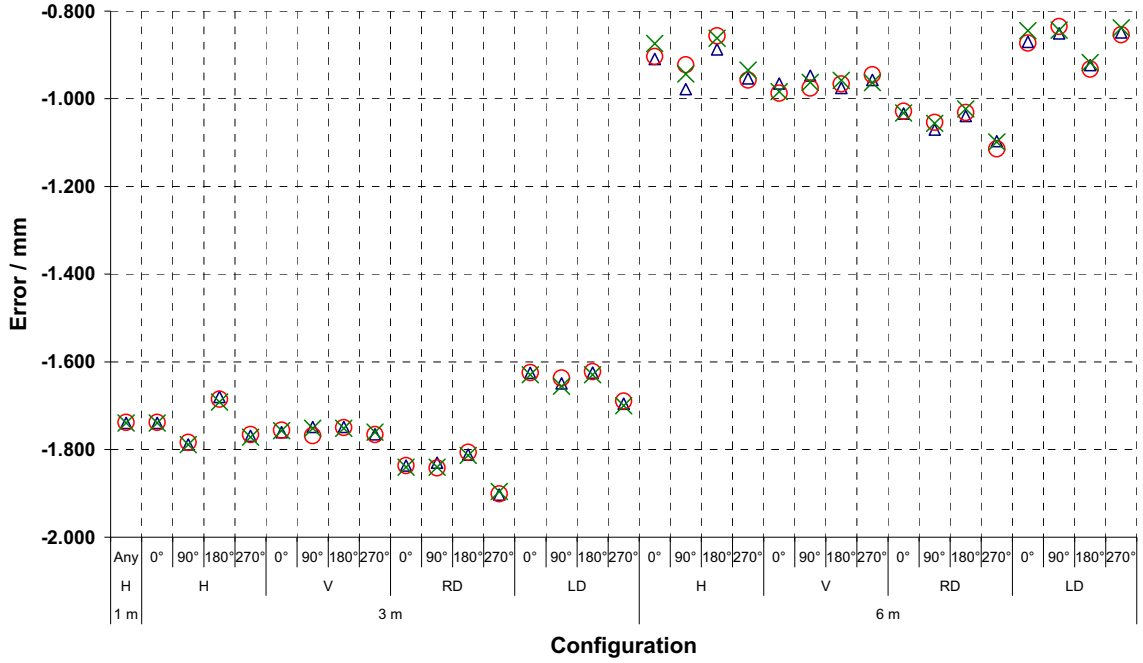

Figure 5. B89 volumetric test results with tracker error map disabled. Configuration parameters are as prescribed in ASME B89.4.19 and relate to three tracker-to-test artefact distances (1 m, 3 m, 6 m) and four azimuth rotations of the tracker (0° to 270°). The orientation of the artefact (horizontal, vertical, and the left and right diagonals) is also indicated. Three measurements are made in each configuration (red circle, green cross, blue triangle).

3.2 Measurement of the target network

Next we set up a network of fixed targets using features usually found in a user's premises, such as the concrete floor, two walls which intersected at a corner and a sturdy stable bench. To support the tracker, we used a commonly available wheeled tripod, a magnetic base and a trivet floor stand. An efficient network design (see §4) consisted of fifteen target holders glued (using a standard hot glue gun) to various locations with five locations for the tracker. Our network used eight target holders glued to the walls, one to the floor and six glued to the bench, at different heights. The laser tracker locations were: two on top of the tripod in the same location but rotated with respect to each other, one on top of the tripod which was extended to full height, one on the bench and one on the floor. The tracker locations were distributed throughout the working volume.

Each target location was measured from all five tracker locations, excluding any targets where line of sight occlusions prevented measurement from a particular tracker position. Each target was measured in front and back sight modes using the IFM. Overall, 126 measurements were made in 55 minutes, including some deliberate repeated measurements of the same target from the same tracker location. Each measurement was made without performing any bundle adjustment or software repositioning of the tracker, so five sets of uncorrected (d, θ, ϕ) data were obtained. Figures 6 and 7 show the relative locations of the five sets of targets with respect to the tracker nominal origin.

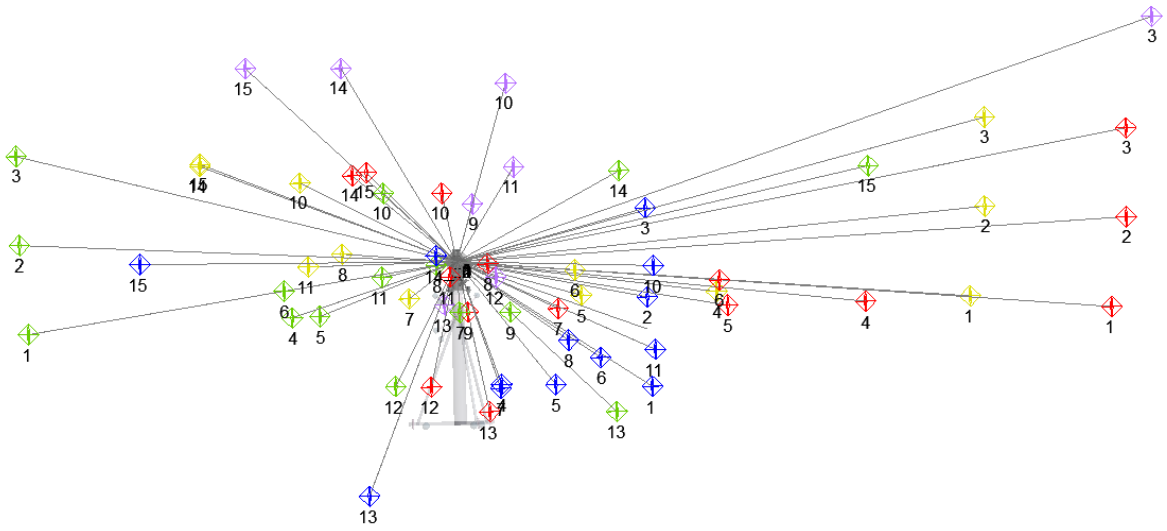

Figure 6. Elevation view of relative position of targets with respect to tracker origin. Target numbers are consistent across the five sets of data.

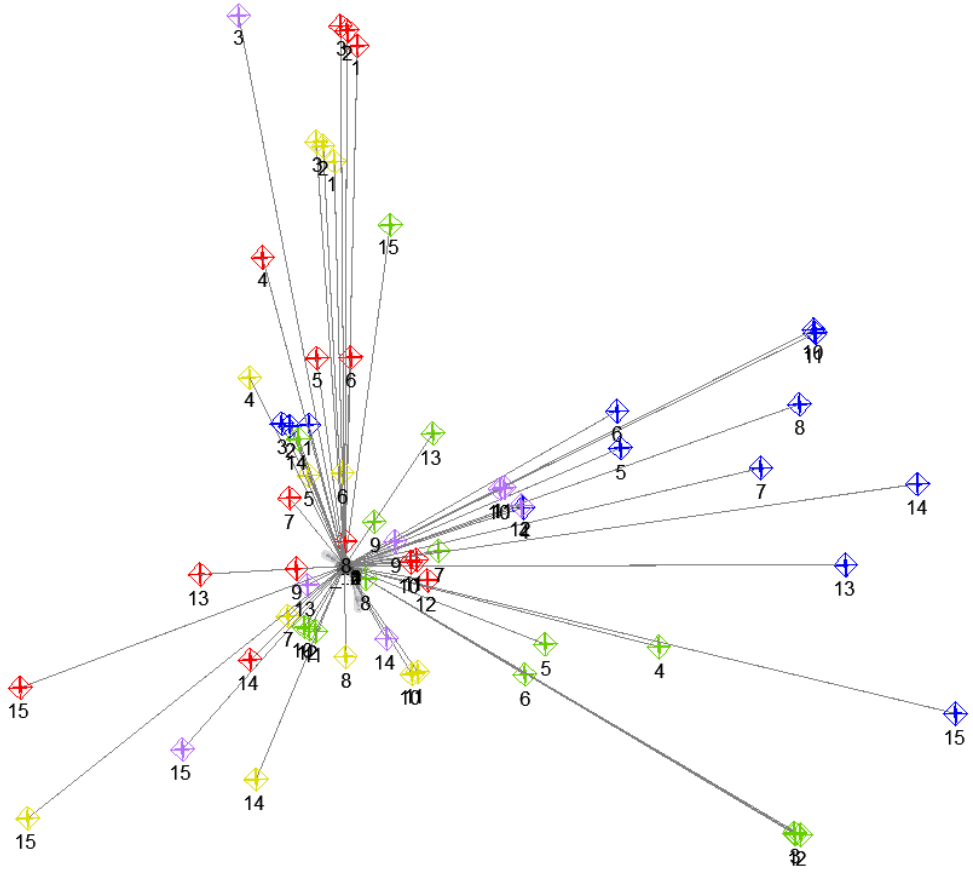

Figure 7. Plan view of relative position of targets with respect to tracker origin. Target numbers are consistent across the five sets of data.

3.3 Results from the model fitting

We used the data obtained from the measurements to solve the least squares problem and obtained the model parameters and their uncertainties. These are reported in tables 2 and 3. In this experiment, we

used the calibrated laser wavelength to set the scale of the system, so defined μ to be zero, with an uncertainty of 5×10^{-7}, corresponding to the uncertainty of the calibrated ranging system.

Table 2. Determined error parameters – distances, scale factor, and their uncertainties. (μ was pre-set).

Symbol	Value	Uncertainty ($k = 1$)
λ	-2.467 6 mm	0.403 µm
μ	0	5×10^{-7}
e_x	4.988 µm	0.122 µm
$b_{y,0}$	91.201 µm	0.654 µm
$b_{z,0}$	-13.318 µm	0.974 µm

Table 3. Determined error parameters - angles and their uncertainties.

Symbol	Value / seconds of arc	Uncertainty ($k = 1$) / seconds of arc
α	16.751	0.128
γ	9.647	0.079
$a_{A,1}$	0.526	0.064
$b_{A,1}$	-0.562	0.080
$a_{A,2}$	0.177	0.073
$b_{A,2}$	1.530	0.090
$a_{E,0}$	0.154	0.223
$a_{E,1}$	-1.736	0.152
$b_{E,1}$	-0.677	0.183
$a_{E,2}$	0.375	0.214
$b_{E,2}$	0.437	0.179

The model solution also provides calculated values for the standard deviations (σ_D, σ_A, σ_E) included in the model equations (3, 4, 5). We use a process of maximising a marginalised posterior distribution to perform *a posteriori* re-weighting of the displacement measurements relative to the angle measurements. This allows us to calculate *a posteriori* values for the noise parameters associated with the distance and angle sensors [13]. The results from the model fitting showed target location standard uncertainties ranging from 2.1 µm to 4.9 µm in magnitude and tracker location standard uncertainties ranging from 1.2 µm to 2.2 µm.

3.4 Using the model to correct the uncompensated tracker

After calculation of the model parameters, we then used our error model to perform *post hoc* correction of the measurements which were previously reported in figure 5. This is equivalent to operating the laser tracker using the NPL error model with values of the error parameters determined from the network test. The results are plotted in figure 8.

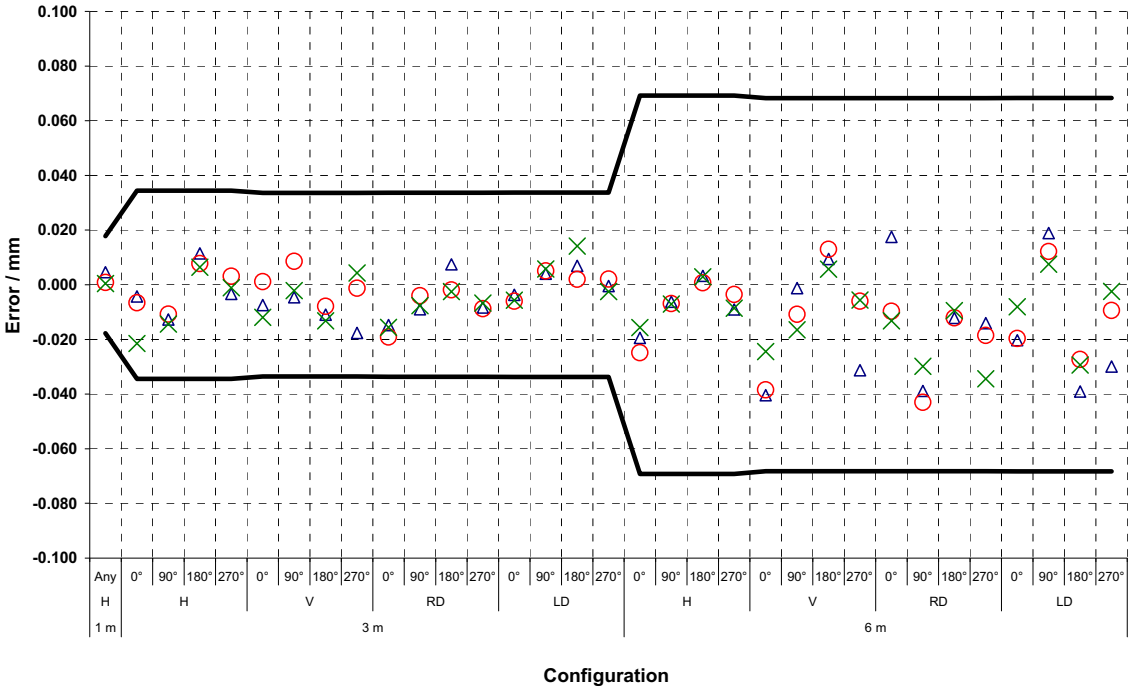

Figure 8. B89 volumetric test results from figure 4, *post hoc* corrected using NPL error model and parameters derived from the network measurement. Bold lines show the manufacturer supplied MPE values.

Figure 8 shows that the performance of the tracker is now well within the MPE values stated by the manufacturer. We then re-instated the manufacturer's error model, ran the manufacturer-specified error determination procedures and re-tested the tracker's performance in the same way as before. The results are plotted in figure 9. The data in figures 8 and 9 are comparable showing that the NPL technique can compensate a tracker as well as the manufacturer's error map. The advantage, however, is that the NPL technique has determined all the error parameters, not just the six which are available for user-determination. One could argue that the data in figure 8 look more consistent and show a smaller spread than those in figure 9 suggesting the NPL technique has performed better – perhaps because it has corrected some additional errors in the angular scales that have occurred since the tracker was manufactured.

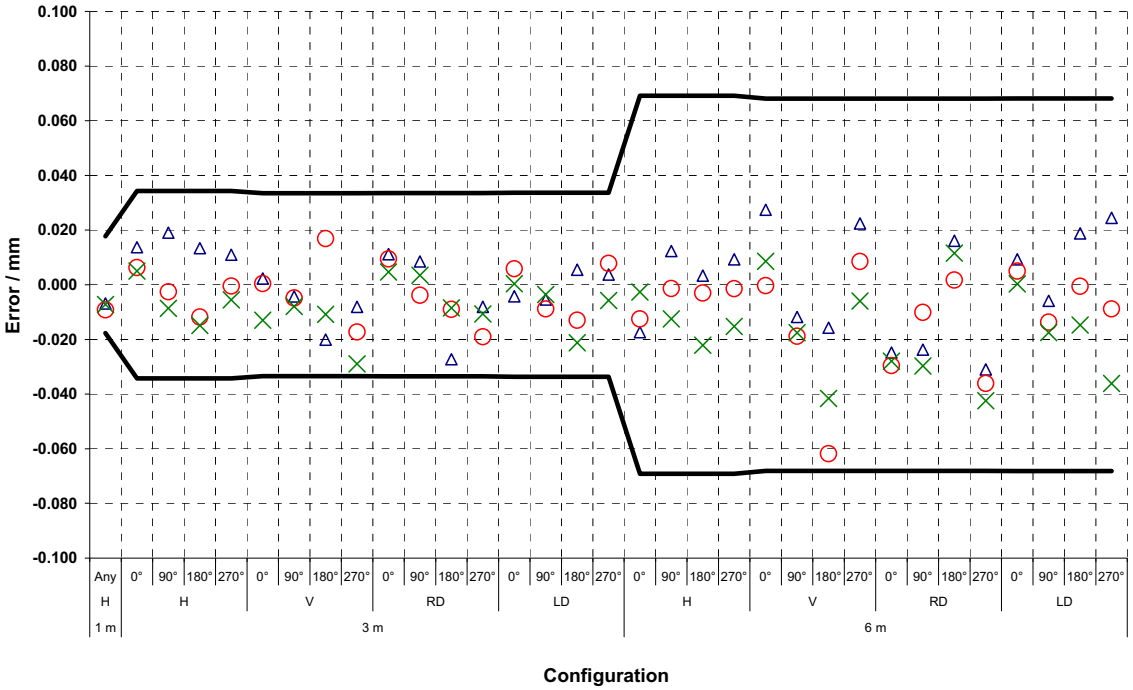

Figure 9. B89 tests using manufacturer's error map. Bold lines show the manufacturer specified MPE values.

4 Target network optimisation

Although our technique will work with almost any reasonable arrangement of target nests, and with more or fewer nests, we spent some time optimising the overall design to achieve sufficient accuracy, whilst minimising the overall number of measurements. The relative locations of the tracker and targets were carefully planned in order to ensure that the whole angular range of the tracker was covered, in both azimuth and elevation; that the target to tracker range varied from the minimum possible to the largest we could accommodate in the available laboratory (~6.4 m); and that two 'birdbath[2] calibration' lines of sight existed, one horizontal, and one on a vertical diagonal.

This last requirement is designed to address one of the issues associated with laser tracker calibration, which is that the birdbath distance (λ) and transit axis offset (e_x) are strongly correlated so that during parameter fitting their combined effect is well determined but the two individual values are poorly separable.

A birdbath calibration is usually performed using two target holders, arranged such that the tracker can measure the target-to-target separation from two locations - outside and inside, on the line joining the two targets (external and internal measurements). For the internal measurement, the tracker has to rotate in azimuth by 180°, whereas during the external measurement the azimuth angle remains fixed - the difference between the two results obtained is due to a combination of λ and e_x. Figures 10 and 11 show, respectively, the internal and external measurements during the birdbath calibration.

[2] 'Birdbath' is a commonly used term which refers to the reference target location that is mounted on a small platform on the side of the laser tracker. The absolute distance from the laser beam origin to this point is a calibration parameter, λ, of the laser tracker error model.

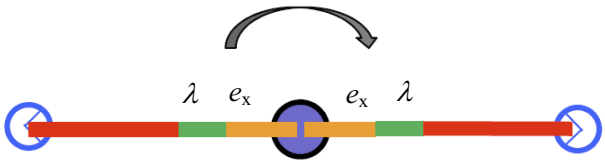

Figure 10. Internal measurement during birdbath calibration. Measurement of the distance to each SMR location is in error by the sum of e_x and λ.

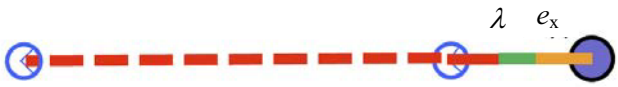

Figure 11. External measurement during birdbath calibration. Measurement of the distance between the SMR locations is unaffected by e_x and λ as they are common to both measurements and therefore cancel.

By adding a second line of sight measurement, which is orientated at a different angle to the vertical (ideally around 45° - see figure 12), the correlation can be broken because λ and e_x have differing dependences on elevation angle.

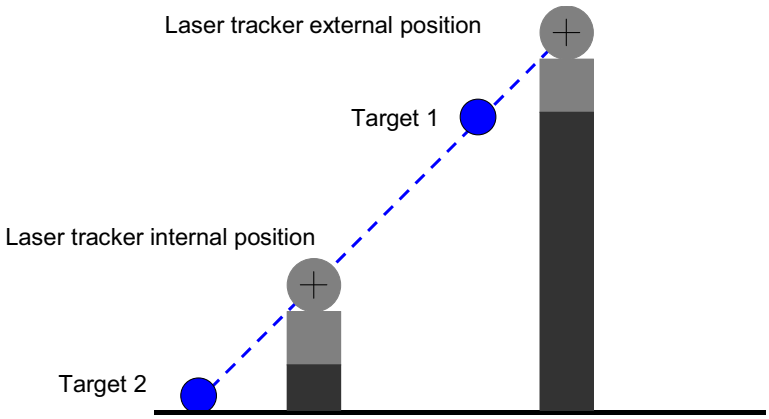

Figure 12 -Measuring the birdbath error using a diagonal line of sight between two targets, set approximately 2 m apart.

It is also important to make measurements in both front and rear face modes, and to include at least two targets (near and far) which are horizontally aligned with the tracker gimbal centre. As shown in figure 13, two-face measurements can also be used to separate λ and e_x, and the vertical diagonal shown in figure 11 is also sensitive, in two-face measurements, to determination of angular offsets such as α, γ, and $a_{E,0}$.

Figure 13. Two-face measurements separate correlated error parameters. In front-face mode (upper), the target range is in error by the sum of e_x and λ., whereas in rear-face mode (lower) the sign of e_x has been reversed.

Using our model, we can also examine any correlations between error parameters by computing the Cholesky factor of the variance matrix. The off-diagonal elements of the Cholesky factor (which is a

lower triangular matrix) indicate the level of correlation between pairs of parameters. We found that the only significant correlations are between γ and b_y, between $a_{E,0}$ and b_z and between $a_{E,2}$ and $a_{E,0}$. The first correlated pair relates to the location of the beam axis **B** in the plane parallel to the *xy*-plane. The second pair relates to the location of the beam axis in the *xz*-plane. The third correlation arises because the elevation angles, ϕ_i, never exceed 57º from the horizontal, so that, for the total set of data, the mean of $\cos(2\phi_i)$ is 0.69. The tracker is mechanically limited to operate over elevation angles from –60° to +77°, so only a small improvement on the achieved elevation angle range could be obtained by placing a target nest high up, close to one of the tracker locations.

5 Conclusions and further work

We have shown how a new network-based error determination can be performed in less than one hour to provide quantitative details of the laser tracker errors (gimbal offsets and misalignments and angular scale errors). The error parameters so determined can be used to predict the performance of the tracker in a verification test, such as that preformed according to ASME B89.4.19. The model parameters are traceable via the laser frequency and the uncertainties of the parameters are determined using rigorous methods. The standard IFM volumetric tests reported in figures 5, 8 and 9 take around two hours to perform and they determine only the magnitude of length measurement errors (and two-face repeatability) of the laser tracker. In contrast, the full ASME B89.4.19 performance verification procedure takes most of one day to perform the volumetric and two-face tests.

At the moment, we are not fully able to perform one-to-one mapping between the NPL error parameters and those of the tracker manufacturer's error map, so we are unable to use our technique to update the error maps in commercial laser trackers directly. This is an area currently under investigation.

The model described in this paper is applicable to most of the currently available models of laser tracker [14, 15, 16], and also to total stations, which have the laser mounted directly on the rotating head. The model does not apply to the older design of tracker [17], which differs mainly from newer designs by having the laser mounted within the tracker body and the laser beam reflected off a gimballed mirror. We are working on some modifications, to adapt the current model to cover the older tracker design.

We are continuing to optimise the design of the network, to minimise the number of measurements required (to reduce the time taken) and to improve the sensitivity to the various error parameters.

Acknowledgements

We would like to acknowledge assistance from Dr Lau and Dr Ma at API Sensor Inc., regarding access to the laser tracker error map, and M Warden for careful reading of the manuscript.

References

[1] Editorial 1984 Documents Concerning the New Definition of the Meter *Metrologia* **19** 163-177

[2] Birch K P, Downs M J 1994 Correction to the updated Edlén equation for the refractive index of air *Metrologia* **31** 315-316

[3] Buscha K, Kunzmann H, Wäldele F 1985 Calibration of coordinate measuring machines *Precision Engineering* **7** 139-144

[4] Hughes E, Wilson A, Peggs G 2000 Design of a high-accuracy CMM based on multi-lateration techniques *CIRP Annals* **49** (1) 391-394

[5] Hughes B, Forbes A, Lewis A, Sun W, Veal D, Nasr K 2011 Laser tracker error determination using a network measurement *Meas. Sci. Technol.* **22** 045103

[6] Hughes B, Sun W, Forbes A, Lewis A 2010 Determining laser tracker alignment errors using a network measurement *CMSC Journal* Autumn 2010, 26-32

[7] Forbes A B 2009 Parameter estimation based on least squares methods *Data Modelling for Metrology and Testing in Measurement Science*, Pavese F, Forbes A B eds., (Birkhauser-Boston, New York) 147–176

[8] Forbes A B, Harris P M 2005 Uncertainty associated with co-ordinate measurements *Laser Metrology and Machine Performance VII* Shore P, ed., (Euspen, Bedford) 30–39

[9] Peggs G N, Maropoulos P G, Hughes E B, Forbes A B, Robson S, Ziebart M, Muralikrishnan B 2009 Recent developments in large-scale dimensional metrology *J. Eng. Manuf.,* B, **223** 571–595

[10] ASME B89.4.19 2006 *Performance Evaluation of Laser-Based Spherical Coordinate Measurement Systems* (New York, USA: The American Society of Mechanical Engineers)

[11] VDI/VDE 2617 part 10 2009 (draft) *Accuracy of coordinate measuring machines: Characteristic parameters and their checking: Acceptance and reverification tests of lasertrackers* (Düsseldorf, Germany: Verein Deutscher Ingenieure)

[12] ISO/NP 10360-10 2010 *Geometrical Product Specifications (GPS) – Acceptance and reverification tests for coordinate measuring systems (CMS) – Part 10: Laser Trackers for measuring point-to-point distances* (Geneva, Switzerland: International Organization for Standardization - new work item proposal)

[13] Forbes A B, Hughes E B, Sun W 2010 Weighting observations from multi-sensor co-ordinate measuring systems *MathMet 2010* (PTB, Berlin)

[14] http://www.apisensor.com/api-laser-tracker-radian-en (visited 29 November 2011)

[15] http://www.faro.com/lasertracker/home/?int_cid=but_uk_trackion (visited 29 November 2011)

[16] http://www.hexagonmetrology.co.uk/leica-absolute-tracker-at401_955.htm (visited 29 November 2011)

[17] http://www.hexagonmetrology.co.uk/leica-absolute-tracker-at901_283.htm (visited 29 November 2011)